Earthquake Engineering & Structural Dynamics
The Journal of the International Association for Earthquake Engineering

EARTHQUAKE ENGINEERING & STRUCTURAL DYNAMICS
Earthquake Engng Struct. Dyn. 2014; **43**:1725–1742
Published online 12 March 2014 in Wiley Online Library (wileyonlinelibrary.com). DOI: 10.1002/eqe.2419

Hybrid simulation testing of a self-centering rocking steel braced frame system‡

Matthew R. Eatherton[1,*,†] and Jerome F. Hajjar[2]

[1]*Department of Civil and Environmental Engineering, Patton Hall, Virginia Tech, Blacksburg, Virginia 24061, U.S.A.*
[2]*Department of Civil and Environmental Engineering, 400 Snell Engineering Center, Northeastern University, Boston, MA 02115, U.S.A.*

SUMMARY

The self-centering rocking steel frame is a seismic force resisting system in which a gap is allowed to form between a concentrically braced steel frame and the foundation. Downward vertical force applied to the rocking frame by post-tensioning acts to close the uplifting gap and thus produces a restoring force. A key feature of the system is replaceable energy-dissipating devices that act as structural fuses by producing high initial system stiffness and then yielding to dissipate energy from the input loading and protect the remaining portions of the structure from damage. In this research, a series of large-scale hybrid simulation tests were performed to investigate the seismic performance of the self-centering rocking steel frame and in particular, the ability of the controlled rocking system to self-center the entire building. The hybrid simulation experiments were conducted in conjunction with computational modules, one that simulated the destabilizing *P-Δ* effect and another module that simulated the hysteretic behavior of the rest of the building including simple composite steel/concrete shear beam-to-column connections and partition walls. These tests complement a series of quasi-static cyclic and dynamic shake table tests that have been conducted on this system in prior work. The hybrid simulation tests validated the expected seismic performance as the system was subjected to ground motions in excess of the maximum considered earthquake, produced virtually no residual drift after every ground motion, did not produce inelasticity in the steel frame or post-tensioning, and concentrated the inelasticity in fuse elements that were easily replaced. Copyright © 2014 John Wiley & Sons, Ltd.

Received 30 July 2013; Revised 21 January 2014; Accepted 17 February 2014

KEY WORDS: seismic design; earthquake resistant structures; self-centering; structural fuses; large-scale experiments; hybrid simulation

1. INTRODUCTION

In the past few years, earthquakes in Japan, Chile, New Zealand, and Italy have caused hundreds of billions of dollars of damage. Financial losses due to earthquakes are exacerbated by the need to demolish buildings that do not collapse and rebuild new structures. For instance, more than 1000 buildings in the Christchurch Central Business District were demolished following the February 22, 2011 Earthquake even though many of them did not collapse [1]. To reduce financial losses due to earthquakes, improve seismic resilience of communities, and enhance sustainability of our built environment, it is necessary to make buildings reusable after large earthquakes.

The self-centering rocking steel frame is a seismic force resisting system that can virtually eliminate permanent drifts after an earthquake and concentrates inelasticity in replaceable elements. The target seismic performance objectives are for the structure to endure a rare earthquake (maximum

*Correspondence to: Matthew R. Eatherton, Department of Civil and Environmental Engineering, Patton Hall, Virginia Tech, Blacksburg, Virginia 24061, U.S.A.
†E-mail: meather@vt.edu

‡This article was published online on 12 March 2014. Errors were subsequently identified in the acknowledgements. This notice is included in the online and print versions to indicate that both have been corrected on 13 May 2014.

considered earthquake (MCE)), subsequently return to plumb, remain safe to occupy, and structurally only require targeted repair. These performance objectives are achieved through a combination of a restoring force mechanism based on structural rocking and replaceable fuse elements that yield, thus protecting the rest of the structure from inelasticity.

More specifically, the self-centering rocking steel frame consists of several basic components that are demonstrated in Figure 1. Stiff steel concentrically braced steel frames are design to remain essentially elastic. The frames are not anchored down to the foundation, but instead are allowed to undergo rigid body rotation about a pivot point at the bottom of one of the columns. Sliding is restrained by bumpers (as shown in Figure 1) or a trough in the foundation. Vertical post-tensioning strands are anchored between the foundation and at the roof level of the braced frame. The post-tensioning strands are stressed to an initial force level, undergo additional elongation as the steel frame rocks, apply a downward force on the frame, and thus produce a restoring force as they act to close the uplifting gap. Steel plates with specially designed cutouts are connected between the two frames and act as shear fuses that are replaceable after an earthquake. The shear fuses are capable of dissipating substantial seismic energy through cyclic yielding.

Figure 1 shows one possible configuration of the system that consists of two rocking steel frames with shear fuses between them. A number of other configurations have been investigated as will be discussed in the background section. However, the mechanics of rocking system behavior are common to almost all of the configurations even if the details are not. The earthquake demands and design capacity of the rocking frame are defined in terms of overturning moment. Because rocking systems are governed primarily by first mode rigid body rotation, the overturning moment is a more important quantity for defining response than base shear. For example, the overturning moment that causes uplift at the base or yielding of the fuses will be relatively constant for different distributions of lateral loads even though the associated base shear will vary.

As the post-tensioned (PT) rocking frame is designed to remain elastic, its behavior, shown in Figure 2(b), is elastic bilinear, in which the overturning moment required to cause uplift, M_{up}, is equal to the initial post-tensioning force, F_{pti}, multiplied by its eccentricity with respect to the pivot point, X_{PT}, plus the expected actual gravity loads, P_{De}, multiplied by their eccentricity with respect to the pivot point, X_D. The secondary slope in Figure 2(b) is due to an increase in the post-tensioning force due to additional elongation during rocking. A well-designed energy dissipating element might be idealized with elastic–perfectly-plastic response as shown in Figure 2(c) with the overturning moment that causes yield, M_{fsy}, equal to the shear yield capacity, V_{fp}, of the fuse multiplied by the eccentricity with respect to the pivot point, X_{fs}, shown in Figure 2(a). Combining the PT frame and the fuse system in parallel, results in the flag-shaped hysteretic behavior shown in Figure 2(d). The nominal resistance to overturning moment, M_y, is given in Eq. (1) as a function of the variables discussed previously and shown in Figure 2(a).

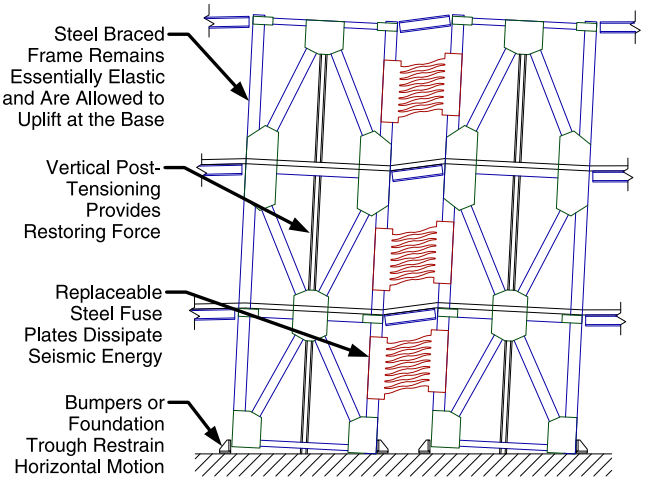

Figure 1. The self-centering rocking steel frame system.

DOI: 10.1002/eqe

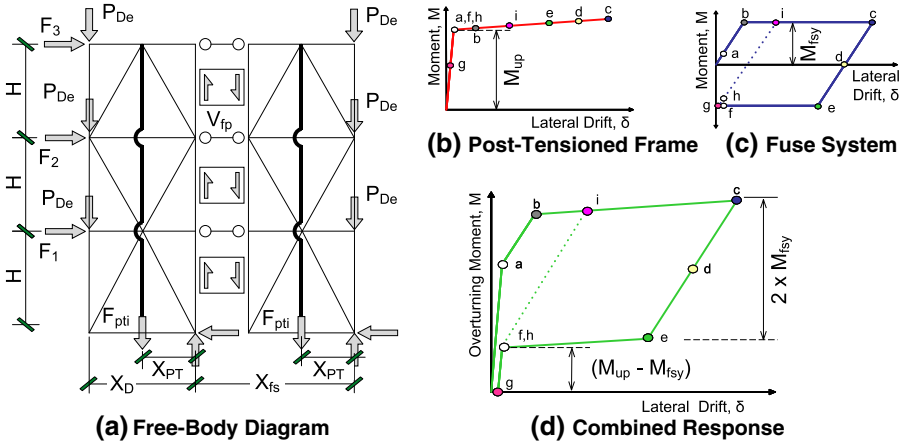

Figure 2. Mechanics of rocking frame behavior.

$$M_y = \sum F_{pti} X_{PT} + \sum P_{De} X_D + \sum V_{fp} X_{fs} \tag{1}$$

The maximum possible residual drift of the rocking frame is readily available from Figure 2(d) as the drift remaining when the applied overturning moment is removed (shown as point g). However, to understand the ability of buildings to self-center in practice requires the consideration of the lateral load resistance of the rest of the building and consideration of dynamic effects. The rest of the building provides additional strength and stiffness that can reduce peak drifts, but after undergoing inelasticity, the rest of the building can create forces that oppose displacements toward zero drift. These actions have conflicting effects on self-centering. To determine whether a building including a self-centering rocking system will actually self-center requires the consideration of the nonlinear resistance of the rest of the building. Furthermore, actual buildings rarely experience the maximum possible residual drifts due to dynamic self-centering effects described further in the next section.

A large-scale experimental program was undertaken to examine the behavior of the rocking steel braced frame system as subjected to severe ground motions. Hybrid simulation testing was used to validate system performance and investigate self-centering ability of the entire three-dimensional structure. Two specimen configurations were tested, each with multiple trials, to vary parameters such as ground motion scale factor, fuse design, inclusion of computational components simulating the resistance of the rest of the building, and addition of out-of-plane displacements. This paper discusses the experimental details, describes the hybrid simulation test setup, presents the results, and presents the conclusions from this experimental program. Other phases of the research project included analysis and testing of the fuse components [2], large-scale shake table tests that investigated dynamic effects such as impact [3], large-scale quasi-static cyclic tests [4], and computational studies [4, 3].

2. BACKGROUND

In the past two decades, several rocking systems have been developed using concrete shear walls and steel braced frames. The precast PT concrete shear walls in Figure 3(a) is similar to the controlled rocking steel braced frame discussed in the previous section with one difference being that energy dissipation is accomplished through special shear yielding connectors between the rocking precast walls [5]. This system was developed as part of the Precast Seismic Structural Systems research program (e.g., [6, 7]) which also developed single precast concrete rocking walls that used mild steel reinforcement at the base of the wall to dissipate seismic energy as shown schematically in Figure 3(b) [8]. Design guidelines and criteria for the precast PT walls are available in American Concrete Institute Innovation Task Group (ITG) [9, 10]. These concepts have also been applied to cast-in-place concrete shear walls [11, 12].

DOI: 10.1002/eqe

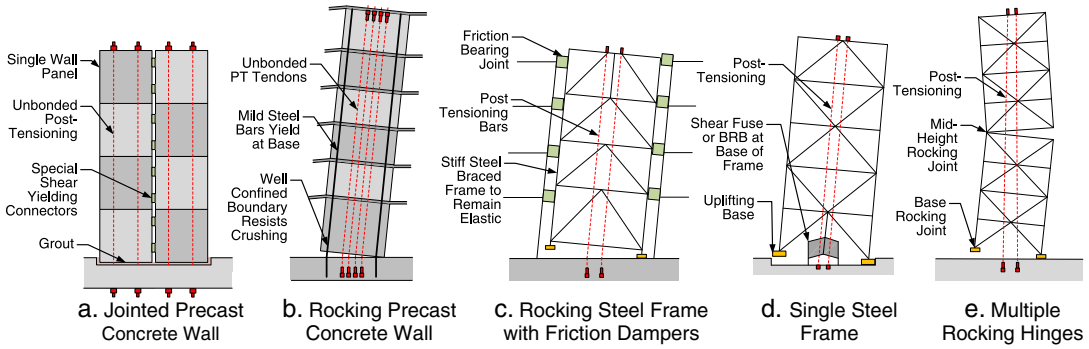

Figure 3. Selected configurations of rocking structural systems investigated in the literature.

Several variations on the steel rocking frame concept have been investigated as early as the 1970s (e.g., [13]) and have ranged from rocking steel bridge piers (e.g., [14]), to yielding uplifting base connections (e.g., [15]) and yielding column splice connections [16]. The rocking frame with friction dampers shown schematically in Figure 3(c) was developed and tested at Lehigh University [17]. This system is unique in the way the lateral load is transferred to the rocking frame through a bearing joint between the rocking frame column and an adjacent column. The bearing connection also dissipates energy through friction in an amount proportional to the magnitude of the bearing force. Single rocking steel frames with energy dissipating devices at the base, such as shown in Figure 3(d), have been investigated using both butterfly fuse plates and buckling restrained braces as the energy dissipating element [3, 4]. Weibe and Christopoulos [18] have tested PT rocking steel frames with multiple rocking sections as shown in Figure 3(e). The additional rocking locations are intended to be an effective way to control seismic force demands in tall frames where higher mode effects are significant.

As described in the previous section, the maximum residual drift a self-centering system by itself is capable of producing can be quantified as the story drift that remains after the lateral loads are slowly removed from the peak drift configuration (point g on Figure 2(d)). However, the actual residual drifts a real building will experience have been shown to be much more complicated. It has been shown that systems with positive kinematic hardening exhibit residual drifts that are well below the maximum possible residual drift [19–22]. MacRae and Kawashima [19] describe the reason as dynamic stability, which occurs at any given time during a displacement history if the yield strength in the direction toward zero displacement has a smaller magnitude than the yield strength in the direction away from zero displacement. Eatherton and Hajjar [23] further studied this concept for seismic force resisting systems with small amounts of restoring force (i.e., self-centering systems that do not fully prevent residual drift). It was found that even small contributions of restoring force result in significant reductions in residual drift and for the configurations studied, it was concluded that if the restoring moment is at least half the yield moment associated with the energy dissipation device, that the system will reliably eliminate residual drifts.

Another potentially important factor in controlling the residual drifts of real buildings is accounting for the nonlinear lateral load resistance of the rest of the building. Common elements of buildings such as interior partitions, steel gravity framing with simple shear beam-to-column connections, stair stringers, and exterior cladding have some ability to resist lateral motion. After these elements deform inelastically during an earthquake, they also create resistance against displacements back to the plumb configuration. In effect, the restoring force has to pull the remainder of the building back to center in order to successfully achieve self-centering capability. Pettinga *et al.* [22] investigated the effect of added lateral load resistance due to gravity framing on reducing peak drifts and thus residual drifts. Eatherton and Hajjar [23] studied the effect of typical interior partitions and typical steel gravity framing on residual drifts of self-centering systems. It was reported that interior partitions provide significant initial lateral load resistance causing a reduction in peak drifts, but then experience severe cyclic strength degradation, which neutralizes their resistance to self-centering. The steel gravity framing retains more cyclic strength and thus can have more effect on residual drift.

DOI: 10.1002/eqe

The hybrid simulation tests described in this paper represent a unique study in which the ability of a physical self-centering system is tested in conjunction with computational components representing the resistance of the rest of the building.

3. EXPERIMENTAL SETUP

The design of the test specimens was based on a prototype building from the SAC studies [24]. The prototype building is three stories tall with typical floor and roof framing shown in Figure 4 and is designed for a site class D location with high seismicity as given by $S_{DS} = 1.00\,\text{g}$ and $S_{D1} = 0.60\,\text{g}$ [25] resulting in a design base shear that was 12.5% of the seismic weight assuming a response modification factor, $R = 8.0$. The seismic masses for the roof and floors were $1033\,\text{kN s}^2/\text{m}$ and $956\,\text{kN s}^2/\text{m}$, respectively. Two dual-frame controlled rocking frame assemblies were assumed in each direction and the large-scale tests represented 0.43 scale relative to one of these prototype frames.

The design overturning moment, M_{ovt}, was calculated as the sum of the equivalent lateral forces, such as those calculated using ASCE 7-10 [25], multiplied by their respective heights above the rocking interface. The resistance to overturning moment was calculated using Eq. (1) with dead load equal to 0, $P_{De} = 0$, and multiplied by an assumed resistance factor, $\phi = 0.9$. The ratio of the design overturning moment, M_{ovt}, to this design resistance, ϕM_y, is given in Table I as the strength ratio for the two specimen configurations. The ability of the system to eliminate drift when the forces are removed is expressed as a self-centering ratio (SC), given by Eq. (2) as the ratio of restoring moment due to initial post-tensioning force, F_{pti}, divided by the resistance opposing self-centering due to the fuse shear capacity, V_{fp}. The dead loads, P_{De}, were set to 0 for the large scale tests. The moment arms, shown schematically in Figure 2(a), were measured to be $X_{PT} = 0.89\,\text{m}$, and $X_{fs} = 2.31\,\text{m}$. Assuming negligible post-tensioning losses, negligible fuse hardening, and ignoring the lateral resistance of the gravity framing, an SC greater than unity will result in near zero drift when the lateral loads are removed. After undergoing inelastic deformations, the gravity framing and nonstructural components act to resist self-centering. Although the effect of post-tensioning losses and fuse hardening can be estimated and if desired, accounted for in Eq. (2), the nonlinear behavior

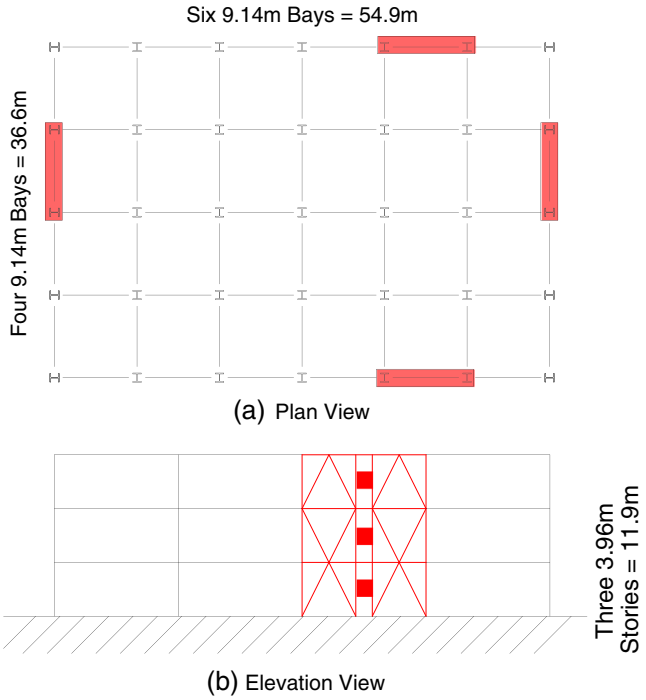

Figure 4. Prototype building.

DOI: 10.1002/eqe

Table I. Testing program for half-scale hybrid simulation tests.

Specimen	Scale levels	System properties	Fuse configuration	Expected fuse behavior	Computational component
A5	MCE (0.69 × Kobe) 1.10 × JMA Kobe 1.10 × JMA Kobe	Strength ratio = 1.12 SC = 1.10	Two 15.9 mm fuses with 8 links V_{fp} = 340 kN	Nondegrading full hysteresis	Leaning column only
A6	MCE (0.69 × Kobe) MCE with OOP* 1.20 × JMA Kobe	Strength ratio = 1.13 SC = 1.10	Six 6.4 mm fuses with 8 links V_{fp} = 349 kN	Degrading pinched hysteresis	Building resistance and leaning column

MCE, maximum considered earthquake; JMA, Japan Meteorological Agency; SC, self-centering ratio.
*10% of in-plane motion concurrently applied in the out-of-plane (OOP) direction.

of the rest of the building including gravity framing with shear connections and interior partitions is not as straightforward. The effect of gravity framing and nonstructural elements such as interior partitions on self-centering ability is therefore investigated separately through computational studies [23] and through hybrid simulation tests described later.

$$SC = \frac{\sum F_{pti} X_{PT} + \sum P_{De} X_D}{\sum V_{fp} X_{fs}} \tag{2}$$

Table I gives information about the six hybrid simulation tests conducted on two specimens. Both specimens were designed using properties that could be considered representative of systems that might be implemented in practice including design overturning moment resistance close to the overturning moment demand assuming $R = 8.0$ and an SC close to 1.0. The two significant differences between specimen A5 and specimen A6 were the fuse type (degrading versus nondegrading behavior) and the type of computational module included (leaning column versus model capturing resistance of the rest of the building). The computational models and scale levels are described further in the following section.

The specimen design is shown in Figure 5(a) and consists of steel wide flange sections turned to have their flanges in the plane of the frame with gusset plates on the front and back. The uplifting

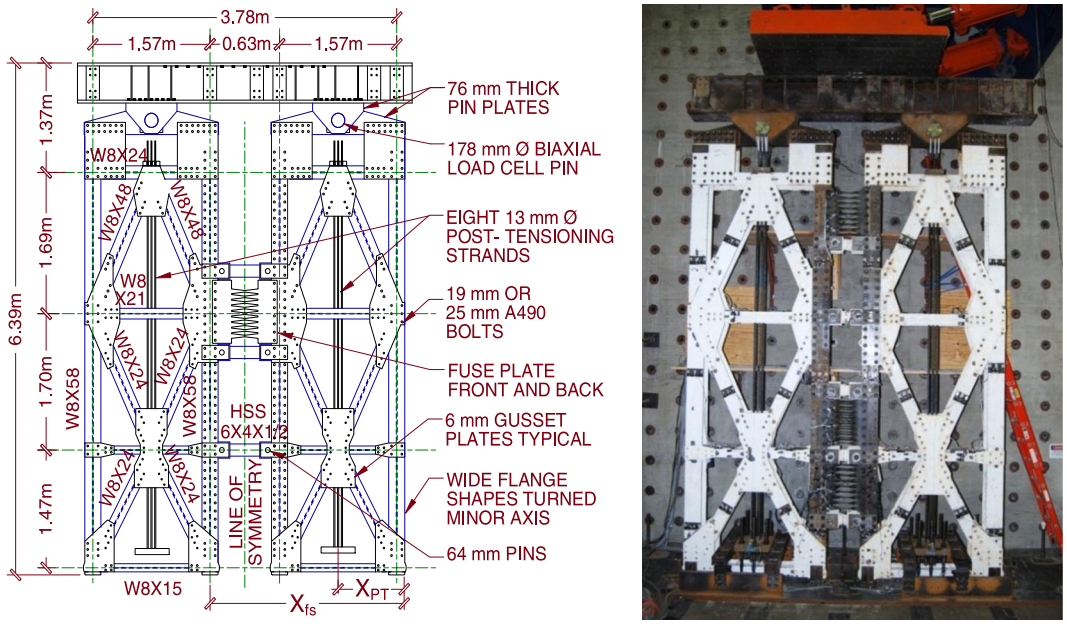

(a) Specimen Details (Specimen A5 Shown)

(b) Photograph of Specimen A6

Figure 5. Specimen layout, dimensions, and photograph.

DOI: 10.1002/eqe

column base is shown in Figure 6(a). The 25 mm thick gusset plates have a rounded edge where they contact the bumpers. The column base plate has a rounded bull nose where it pivots on the base plate below. The same two frames and post-tensioning strands were used for both specimens, and, as intended for use in practice, the only modification made between specimens was replacing the damaged fuse plates. Tube section struts connected the two frames to resist the inward pull of the fuses and to simulate the possible restraint created by a floor slab. They were designed to be elastic and experimental data showed they remained elastic throughout the testing program. The top of the post-tensioning strands were anchored to a 57 mm thick anchorage plate with two part wedges in a conical shaped hole as shown in Figure 6(b). Post-tensioning chucks were used at the bottom. The initial post-tensioning stress was 34% of the guaranteed ultimate tensile strength for both specimens, which corresponds to an initial post-tensioning force of 497 kN in each frame. The yield strength and ultimate strength of the post-tensioning strand was measured based on three tension tests in accordance with ASTM Standard A370-07a to be 1757 and 1956 MPa, respectively.

The fuses, shown in Figure 7, are steel plates with diamond shaped cutouts that are designed to promote the initiation of yielding and plastic hinging at the quarter point away from locations of discontinuities. As such, large ductility is possible and thicker fuse plates can develop full hysteretic behavior. Thinner fuse plates experience lateral torsional buckling of the links, which leads to

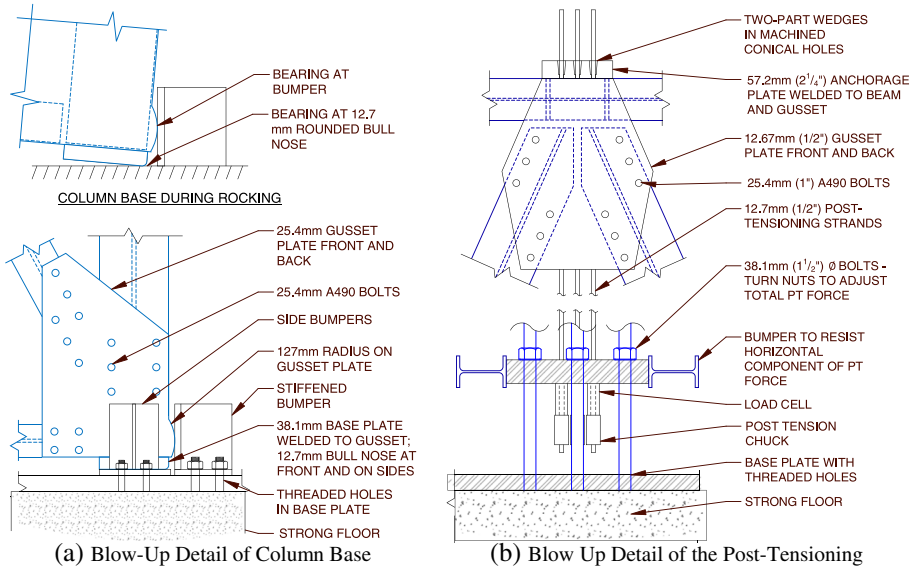

(a) Blow-Up Detail of Column Base (b) Blow Up Detail of the Post-Tensioning

Figure 6. Details of specimen construction.

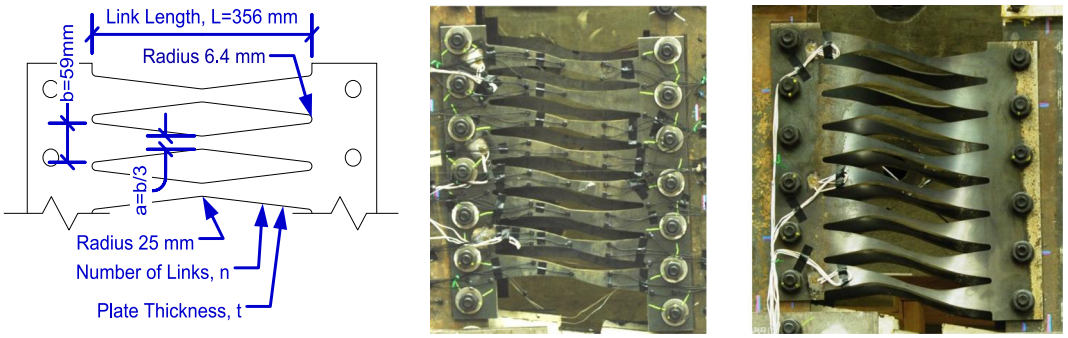

(a) Specimen A5 fuse (b) Specimen A6 fuse during testing (c) Degrading Fuse

Figure 7. Fuse geometry and deformed shape of (a) Specimen A5 fuse – geometry of fuse links and (b) Specimen A6 fuse during testing – nondegrading and degrading fuses.

DOI: 10.1002/eqe

strength degradation. Nondegrading thick fuses can be desirable for their ability to dissipate seismic energy, whereas degrading fuses can be desirable because their resistance against restoring forces degrades leading to improved self-centering ability. Specimen A5 and A6 fuses were designed to develop nondegrading or degrading response by varying the thickness from 15.9 to 6.4 mm for Specimen A5 and A6, respectively. The mean yield stress of the ASTM A36 plate material was measured using four tension coupons for the 6.4 mm plate and three coupons for the 15.9 mm thick plate to be 274 and 317 MPa, respectively. More information on design and behavior of butterfly steel fuse plates can be found in Ma *et al.* [2] and Eatherton and Hajjar [4].

A photograph of a test specimen is shown in Figure 5(b). The top of the loading beam is connected to a Loading and Boundary Condition Box (LBCB) capable of controlling all six degrees of freedom. The loading beam was connected to the two frames through bidirectional load cell pins. The tests were controlled to maintain zero vertical force in the load cell pins and apply the displacements computed by the hybrid simulation time stepping algorithm at the roof level based on the feedback of two string potentiometers. The out-of-plane degrees of freedom were controlled to have zero displacement or rotation except for one trial for Specimen A6 that was controlled to include out-of-plane displacement. Approximately 500 channels of data were recorded for each test including string potentiometers, linear potentiometers, load cells, strain gages, linear variable differential transformers, and Krypton LEDs as well as video cameras and digital still cameras. Additional information on instrumentation can be found in Eatherton and Hajjar [4].

4. HYBRID SIMULATION TEST SETUP

Hybrid simulation tests were used to investigate the performance of the self-centering rocking steel frame system subjected to real ground motions in the presence of second-order gravity load effects and the ambient building resistance. In this paper, ambient building resistance refers to the lateral load resistance of building components not typically included in computational models of the lateral load resisting system.

Two computational models were created using the OpensSEES software [26] to represent the gravity load second-order effects and the ambient building resistance. These computational components were linked to the experimental setup by using the UI-SIMCOR software [27], as schematically demonstrated in Figure 8(b). Test A5 included only one computational component that represented second-order gravity effects, whereas Test A6 also included a computational component representing ambient building resistance of the rest of the three-dimensional structure as shown in Figure 8(b).

The second-order gravity effects were modeled as a pinned-base leaning column with an effective gravity load lumped at the top. The effective gravity load was found by determining the amount of force that caused the same amount of P-Δ moment in the SDOF system as three floors of tributary gravity load [$F = (\sum F_i h_i)/H$]. The tributary mass associated with the SDOF system was computed as the mass that produced the same overturning moment as the three degree of freedom system when

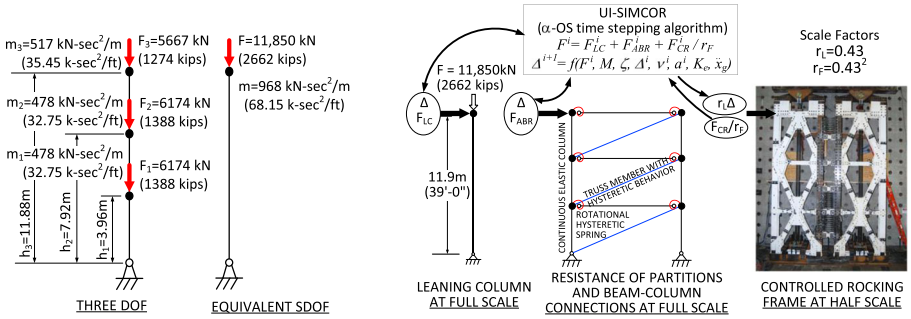

(a) Conversion of 3DOF System to SDOF (b) Schematic Hybrid Simulation Setup

Figure 8. Leaning column and hybrid simulation setup.

DOI: 10.1002/eqe

subjected to a unit acceleration [$m = (\sum m_i h_i)/H$]. The equivalent gravity load and tributary mass are shown in Figure 8(a).

The second computational model simulated two of the largest contributors to ambient building resistance, namely wall partitions and gravity framing with simple shear beam-to-column connections. As shown in Figure 8(b), the simple shear beam-to-column connections were modeled as rotational springs between the beams and columns of a one bay frame. A rotational spring was calibrated to match an experimental test conducted by Liu and Astaneh [28] on a simple shear connection between a W18x35 beam composite with a 152 mm lightweight concrete slab on metal deck to a W14x90 column using a single shear plate with four 22 mm diameter A325 bolts [28]. The experimental and calibrated responses are shown in Figure 9(a). The prototype building shown in Figure 4 has a total of 30 gravity beams oriented in the longitudinal building direction between columns, which after subtracting two bays of rocking frames and dividing by two, leaves 14 bay of gravity framing tributary to each rocking frame. The backbone moments were, therefore, amplified by a factor of 14 to simulate the 14 tributary gravity framing bays.

The partitions were represented by a nonlinear hysteretic truss element that were calibrated to match experimental tests conducted by Gad *et al.* [29] on 2.4 × 2.4 m typical cold-formed steel partitions with 10 mm gypsum board on two faces attached with 25 mm long number 6 screws at 200 mm vertical edge spacing, 600 mm top and bottom edge spacing, and 400 mm field spacing. The comparison of experimental and calibrated response is shown in Figure 9(b). The backbone forces were amplified by a factor equal to 9.14 m/2.4 m × 14 bay to simulate the resistance of a total of 9.14 m of partition wall in each of the 14 tributary bays. For the sake of simplicity, exterior partitions were assumed to have identical response to interior partitions.

The Japan Meteorological Agency JMA Kobe ground motion, shown in Figure 10(a), was used to allow direct comparison with related shake table tests performed at the E-Defense facility in Miki, Japan [3]. Whereas the hybrid simulation tests were conducted at a quasi-static testing rate, the shake table tests by Ma *et al.* [3] were able to investigate dynamic effects such as determining that impact does not have

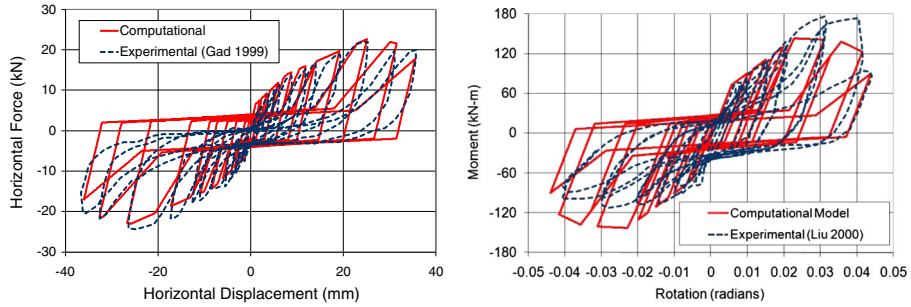

Figure 9. Calibration of the gypsum board on metal stud partition response (left) and the shear beam-to-column connections (right).

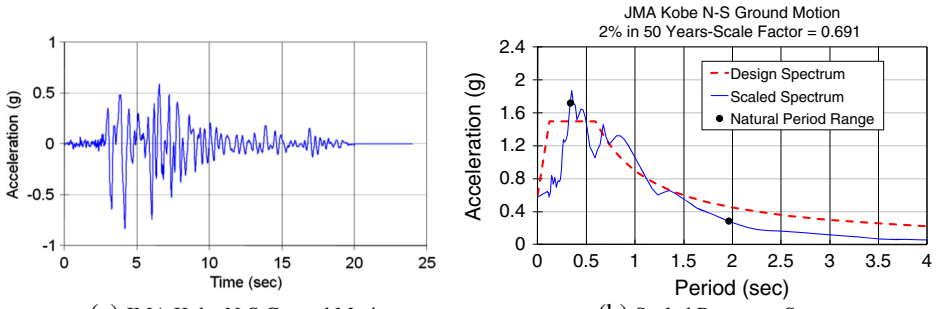

(a) JMA Kobe N-S Ground Motion (b) Scaled Response Spectrum

Figure 10. Japan Meteorological Agency JMA Kobe N-S ground motion and associated pseudo-acceleration response spectrum scaled to 2% in 50 years hazard level with scale factor 0.69.

DOI: 10.1002/eqe

a significant effect on peak frame member forces. The ground motion was scaled to best match the design spectrum by using a least squares method over a period range of interest (0.34 to 2 s), which represents the initial elastic period up to the maximum expected period calculated using the secant stiffness at peak expected drift. The design response spectrum and scaled spectrum are shown in Figure 10(b). Multiple trials were conducted for both Specimens A5 and A6 including trials at the MCE level corresponding to a scale factor of 0.69 and scale factors of 1.10 and 1.20 for Specimens A5 and A6, respectively. As given in Table I, one of the hybrid simulation tests for Specimen A6 also included the application of out-of-plane motion equal to 10% of the in-plane displacements, the magnitude of which was selected on the basis of physical limitations in the test setup.

The hybrid simulation test procedure is demonstrated schematically in Figure 8(b) as managed by the hybrid simulation software UI-SIMCOR. For each hybrid simulation trial, the computational modules were started from an undamaged condition, meaning that the strength and stiffness degradation in the gravity connections and interior partitions was not carried over from previous trials. The displacement for the current time step, Δ, is applied to both computational components, and a displacement reduced by the length scale factor, $r_L = 0.43$, is applied to the experimental setup. The resulting forces are measured, the experimental force is divided by the force scale factor, $r_F = 0.43^2$, and the forces are summed together. The displacement for the next time step is calculated using the α-OS time-stepping method [30] based on the measured force, F^i, computationally applied mass, M, computationally applied damping, $\zeta = 0.02$, velocity, v^i, acceleration, a^i, an elastic stiffness, K_e, and the current ground acceleration, $\ddot{x}_g^i$.

5. COMPUTATIONAL MODELING

A two-dimensional nonlinear analysis model of the specimen was created using the OpenSees software [26] including the effects of geometric and material nonlinearity. The frame members shown in Figure 11(a) were simulated using elastic frame elements. At the base of the frames, gap elements, near rigid in compression with zero stiffness in tension simulated the compression-only support and bumpers, these gap elements were oriented in both the horizontal and vertical directions. The model was built in stages to simulate expected construction sequencing. The fuse elements were not created until the initial PT forces were equilibrated through the frame. The struts that connect the two frames utilized an elastic–perfectly-plastic constitutive relationship with a truss element, but were not found to experience yielding in any of the computational simulations of the tests or in the experimental program. The pin connections at each end of the struts were modeled as shown in Figure 11(a) and blown up in Figure 11(b). The pin holes each had approximately 1.6 mm tolerance greater than the pin, which had a cumulative effect resulting in a total of 6.4 mm displacement

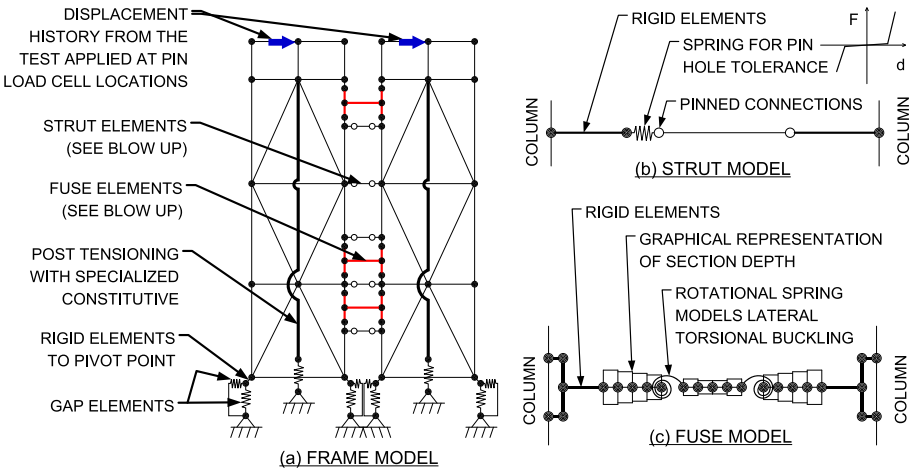

Figure 11. Computational model of the controlled rocking system.

DOI: 10.1002/eqe

required to go from axial tension to axial compression or vice versa. This lag was modeled using a zero length spring that represented the pin hole tolerance as shown in Figure 11(b).

A phenomenological model was created to simulate the flexural, axial, and lateral-torsional buckling behavior of the fuse links that interact to create the unique shear force – shear distortion response of the fuse plates. As shown in Figure 11(c), the fuse was modeled with 12 fiber section elements using a formulation that neglects shear deformations on the element level. The depth of the fiber section matched the average depth of the fuse link along that portion of its length. The thickness of the section was set equal to the thickness of the fuse plate multiplied by the number of links being represented. The material constitutive for the fuse used the Giuffre–Menegotto–Pinto model with the measured yield stress and a combination of isotropic and kinematic hardening as demonstrated later in Figure 17(a). Rotational springs were included at the third points of the fuse link to simulate lateral-torsional buckling. The rotational spring was a zero-length element with a cyclic behavior using the Pinching4 material in OpenSees. It had a steep initial stiffness up to a lateral-torsional buckling critical moment as shown in Figure 17(b), and then the ability of the spring to resist moment was significantly reduced. The critical buckling moment was computed using a relationship defined in Eatherton and Hajjar [4] relating the experimentally obtained buckling shear forces with fuse link slenderness.

For most specimens, the constitutive model used for the post-tensioning was essentially bilinear with modulus of elasticity equal to 202 GPa, a yield stress equal to 94% of the nominal ultimate stress and a post yield stiffness equal to 1.7% of the initial modulus of elasticity.

6. RESULTS AND DISCUSSION

6.1. Specimen A5 behavior

The displacement response of specimen A5 to the MCE scaled ground motion is shown in Figure 12(a) and the corresponding load-deformation behavior is shown in Figure 12(b). As mentioned at the beginning of this paper, the overturning moment is a better measure of earthquake demand and design capacity than base shear because the rocking systems are governed by rigid-body rocking behavior. Thus the vertical axis on Figure 12(b) is the applied overturning moment normalized by the design overturning resistance computed using Eq. (1). Figure 12(b) shows that Eq. (1) is relatively accurate in predicting the overturning moment capacity of the system.

The peak drift is tabulated in Table II to be 1.7% roof drift. The maximum possible residual roof drift for the hysteretic shape shown in Figure 12(b) is the width of the hysteresis loop for zero overturning moment equal to 0.3% roof drift. However, as shown in Figure 12(a), the actual residual drift was found to be negligible (0.0%). The maximum possible residual drift is controlled by the system proportioning as

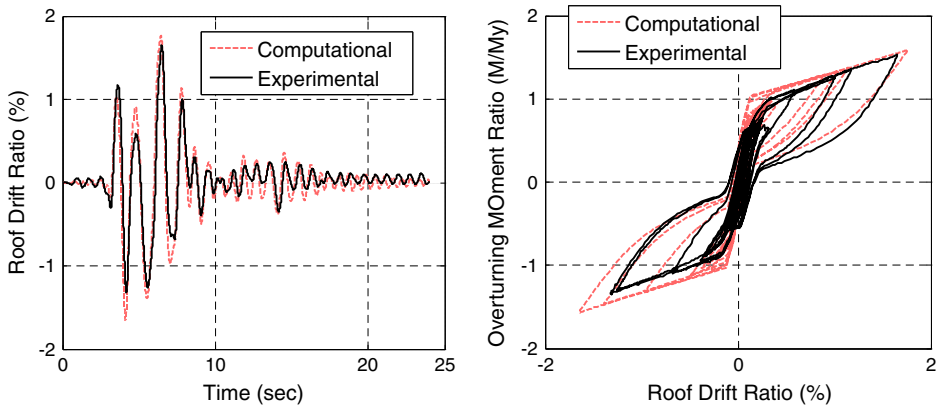

(a) Displacement History (b) Load-Deformation Response

Figure 12. Response of Specimen A5 to the ground motion scaled to maximum considered earthquake level.

DOI: 10.1002/eqe

Table II. Summary of drifts during the hybrid simulation tests.

Specimen	Scale level	Experiment peak roof drift ratio (%)	Time at peak roof drift (s)	Computational model peak roof drift ratio (%)	Time at peak roof drift (s)	Percent difference in peak drift (%)	Experimental residual roof drift (%)
A5	MCE	1.7	6.49	1.8	6.43	7	0.0
A5	1.10 × Kobe Trial 1	2.4	6.55	2.8	6.50	15	0.0
A5	1.10 × Kobe Trial 2	2.6	6.60	2.8	6.50	6	0.0
A6	MCE	1.4	4.10	1.7	4.10	23	0.0
A6	MCE with 10% OOP	1.5	4.08	1.7	4.10	13	0.1
A6	1.20 × JMA Kobe	2.5	5.59	3.3	6.47	30	0.0

MCE, maximum considered earthquake; JMA, Japan Meteorological Agency; OOP, out-of-plane.

represented by the SC, SC = 1.10. The actual residual drifts are often much smaller than the maximum possible residual drifts in systems that have any restoring force component due to increased probability of yielding toward zero displacement as described in the background section. The hysteretic energy dissipation is also related to the SC and because the SC is just slightly larger than unity, the hysteretic energy is shown to be approximately the largest flag shape area possible while still limiting the roof drift when the overturning moment is removed.

The energy dissipation in the global response is almost entirely due to energy dissipation in the fuses shown in Figure 13(a). The horizontal axis in Figure 13(a) is the fuse link shear strain, calculated as the shear deformation of the fuse divided by the link length, *L*. The vertical axis is the shear force normalized to the calculated fuse shear capacity reported in Table I. Figure 13 demonstrates the typical behavior of a nondegrading fuse that produces full hysteretic behavior. The peak shear strain across the fuse link during the hybrid simulation was 8%, which was considerably less than the shear strains that were found to cause fracture in component tests (30–42%) [2]. Furthermore, the component tests on fuses showed that the butterfly fuse plates can undergo considerably more inelastic cycles and cumulative strain than what is shown in Figure 13(a).

The computational model curves shown in the results plots were obtained by substituting the computational model shown in Figure 11 for the experimental module in the hybrid simulation test setup. The computational model is shown in Figure 12 to slightly overestimate the displacement in the hybrid simulation experiment. Peak displacements are summarized in Table II showing the peak displacement was overestimated by 7%, and the time at peak displacement was within 0.06 s of the experimentally observed peak. Although the computational model was shown to capture the character of the experimental response as shown in Figure 12(b), several secondary behavioral

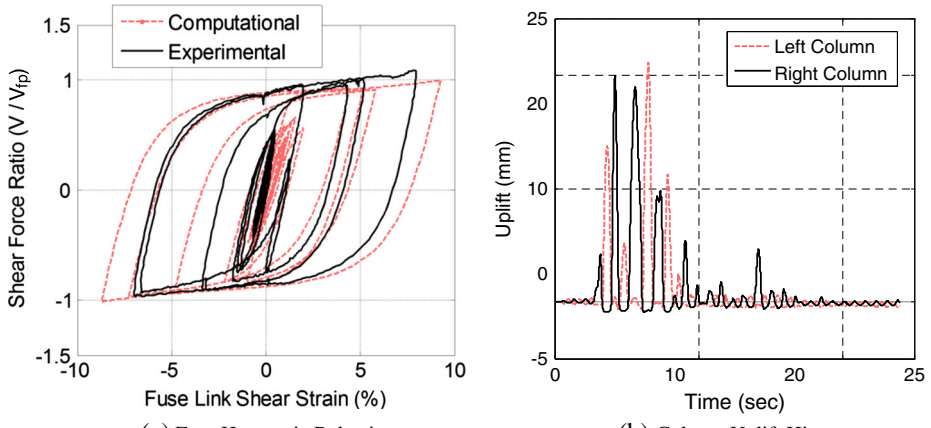

(a) Fuse Hysteretic Behavior (b) Column Uplift History

Figure 13. Fuse and uplift behavior of Specimen A5 for the maximum considered earthquake ground motion.

DOI: 10.1002/eqe

phenomena contributed to differences. The idealized initial system behavior has sharp transitions in stiffness as shown in Figure 2(d) although uneven bearing between rocking columns in the actual specimen caused lower initial stiffness and a rounding of these sharp transitions as demonstrated in the experiments and supported by analysis in Eatherton and Hajjar [4]. The computational modeling also did not incorporate some sources of flexibility such as sliding at the base of the frames, which is evidenced by horizontal shifts in the experimental response at $0.6M_y$ shown in Figure 12(b) or flexibility of the PT connection to the strong floor associated with the base assembly shown in Figure 6(b). The sliding was measured to be approximately 5 mm for both Specimens A5 and A6. Figure 13(a) shows that the computational model of the fuse captured the strength and stiffness of the fuse well.

Figure 13(b) shows the uplift history for both column bases of the right frame. The peak uplift is shown to be 21 mm, which is well within the design maximum uplift accommodated by the bumpers that is more than 100 mm. Figure 13(b) shows that at the end of the ground motion, both columns come to rest with near zero uplift. It can also be demonstrated using the uplift data that the uplift ratio calculated as the uplift divided by the distance to the pivot point is almost identical to the roof drift ratio implying that the frame undergoes rigid body rotation with negligible elastic deformations.

Because the performance at the MCE level was more than satisfactory, two trials were performed at a larger scale level. The scale level was increased from 0.69 for the MCE level event to 1.10 or 69% larger than the MCE motion. Two trials were conducted with the same earthquake ground motion and scaling to investigate degradation in the system performance. The load-deformation response for both trials is shown in Figure 14(a), and the fuse behavior is shown in Figure 14(b). As shown, there was almost no degradation in behavior between the trials. There was an 8% increase in the peak displacements listed in Table II from one trial to the next. The fuse behavior shown in Figure 14(b) did not appear to degrade at all. The peak shear strain across the fuse link was 15%, which was still only half the shear strain that caused fractures in the tests by Ma *et al.* [2]. In short, Specimen A5 was subjected to three infrequent and large earthquake ground motions without any repairs in between, and the residual roof drift ratio was 0.0% after every run, and no inelasticity was observed outside the fuses. This implies that a well-designed self-centering rocking frame system may not need structural repairs, nor even need to have the fuse replaced after a large earthquake.

6.2. *Specimen A6 behavior*

Specimen A6 used thinner degrading fuse plates and included the computational modules simulating ambient building resistance. As shown in Figure 15, the peak displacements for a trial with a 1.20 scale factor produced similar peak displacements as the Specimen A5 nondegrading fuse

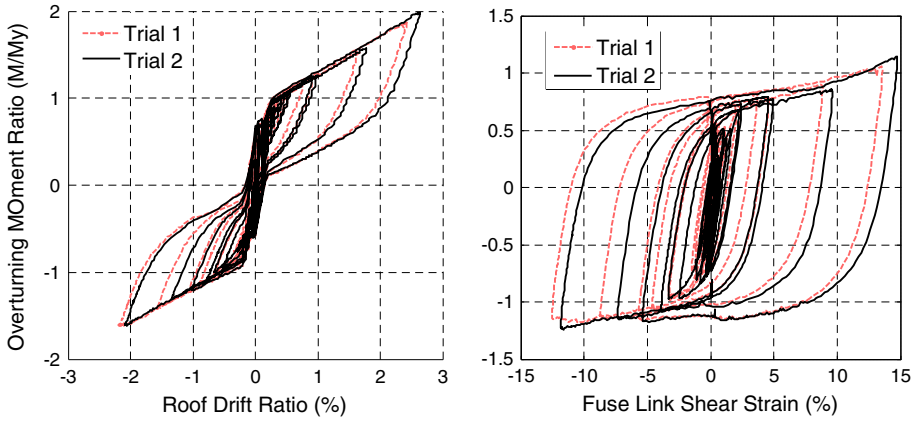

(a) Load-Deformation Response (b) Fuse Hysteretic Response

Figure 14. System and fuse response for Specimen A5 subjected to two trials of the JMA Kobe ground motion scaled by 1.10.

DOI: 10.1002/eqe

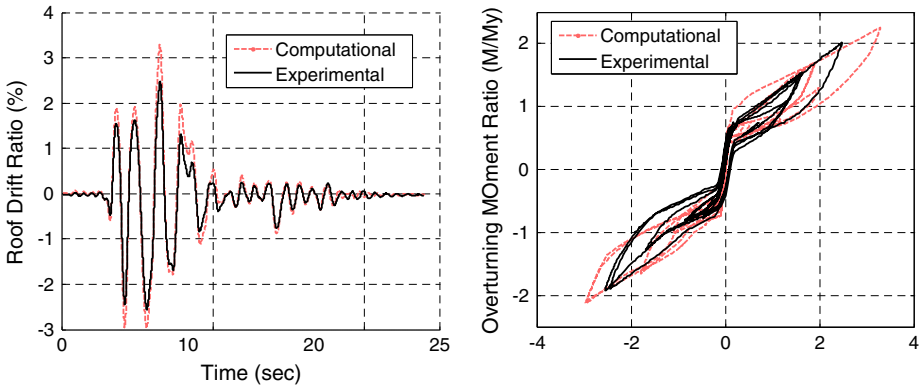

(a) System Displacement History (b) Load-Deformation Response

Figure 15. Response of Specimen A6 to the Japan Meteorological Agency JMA Kobe ground motion scaled by 1.2.

configuration subjected to the Japan Meteorological Agency JMA Kobe ground motion with a 1.10 scale factor. There are several factors that affect the peak drifts of Specimen A5 as compared with Specimen A6. First, the peak drifts were reduced because of the added resistance provided by the rest of the building. It is shown in Figure 16 that the ambient building resistance reached an overturning moment resistance equal to the design overturning capacity of the rocking frame system, M_y. This significant addition of resistance surely caused reduction in the peak drifts. However, the reduced energy dissipation associated with fuse degradation likely counteracted this effect as the hysteretic damping was significantly reduced.

The reduction in energy dissipation capacity is demonstrated by the shape of the hysteresis loops. The height of the self-centering flag is reduced by approximately 50% compared with the nondegrading Specimen 5 that has a similar SC. Some guidance for minimum energy dissipation in self-centering systems is provided in Seo and Sause [31] and the American Concrete Institute [9]. Figure 15(b) shows the response of the system after two previous tests at the MCE level in which the fuse buckled and began degrading. The response shown in Figure 15 demonstrates that the self-centering rocking frame system with a degrading fuse was able to survive three large earthquakes ground motions and still limit peak drifts and eliminate residual drifts.

Ambient building resistance is expected to have two opposing effects on self-centering. First, the peak displacements are reduced because of the added lateral load resistance. Because the peak drifts

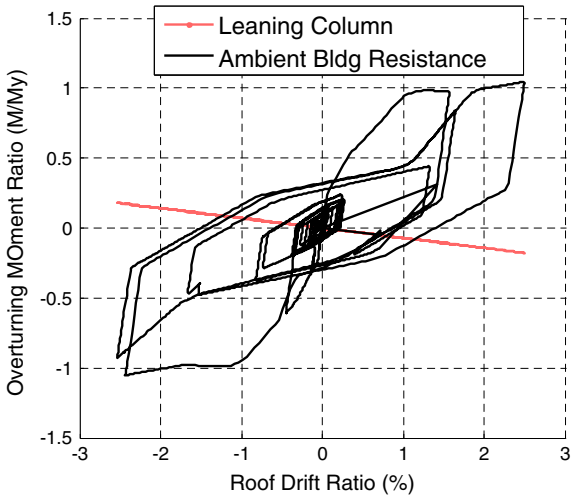

Figure 16. Computational component responses for Specimen A6 subjected to Japan Meteorological Agency Kobe ground motion scaled by 1.2.

DOI: 10.1002/eqe

for Specimen A6 were also increased due to smaller hysteretic damping compared to Specimen A5, and both specimens had computationally modeled P-Δ, which increases peak drifts, the effect of ambient building resistance on peak drifts were not directly obtained from the test results. On the other hand, the ambient building resistance resists the ability of the self-centering system to return to plumb, which may cause an increase in residual drifts. However, Figure 16 demonstrates that the ambient building resistance strength deteriorates rapidly. This is due to concrete crushing in the composite beam-column connections and ovalization around screw holes and other damage to interior partitions. At the end of the test, the force created by the ambient building component degraded to approximately 10% of its initial strength as the frame passed through zero displacement. This implies that as the restoring force brought the building back to plumb (zero drift) that the rest of the building was not providing much resistance by the end of the test.

The computational model for the degrading fuse reached its critical moment as shown in Figure 17 (b) and thus simulated strength loss due to lateral torsional buckling of the butterfly links. The rotational springs at both ends reached their critical moment and subsequently retained only a fraction of their prebuckling moment capacity. However, the limitations of using a pinching hysteretic model in a rotational spring to model lateral torsional buckling include that buckling is related only to a critical moment instead of an axial-moment interaction (or other possible criteria), the unloading and reloading rules in the hysteretic models available in OpenSees may not accurately represent lateral torsional buckling behavior, and calibration of this type of model requires many tests to define buckling parameters for a range of butterfly link geometries and thicknesses. The constitutive model and hardening rules used for the butterfly link fiber sections demonstrated in Figure 17(a) were capable of capturing prebuckling behavior well as discussed previously for Specimen A5.

As listed in Table I, the second trial for Specimen A6 included the application of out-of-plane motion with a magnitude equal to 10% of the in-plane displacements. The objective of this hybrid simulation test was to investigate the behavior of the rocking frame system when subjected to loading not parallel to the building axis or as subjected to torsion associated with eccentric loading. It was found that the peak displacement, peak force, time of peak displacement, and dissipated energy were 9% larger, 1% smaller, approximately the same, and 11% smaller, respectively, as compared with the trial without out-of-plane motion. Because the differences can be explained by strength degradation in the fuses from one test to the next, it is likely the out-of-plane motion has negligible effect on in-plane hysteretic behavior. In all hybrid simulation tests, including the second trial for Specimen A6, the braced steel frame and post-tensioning remained elastic. The condition of the bearing surfaces at the rocking interface was inspected after testing, and no evidence of bearing

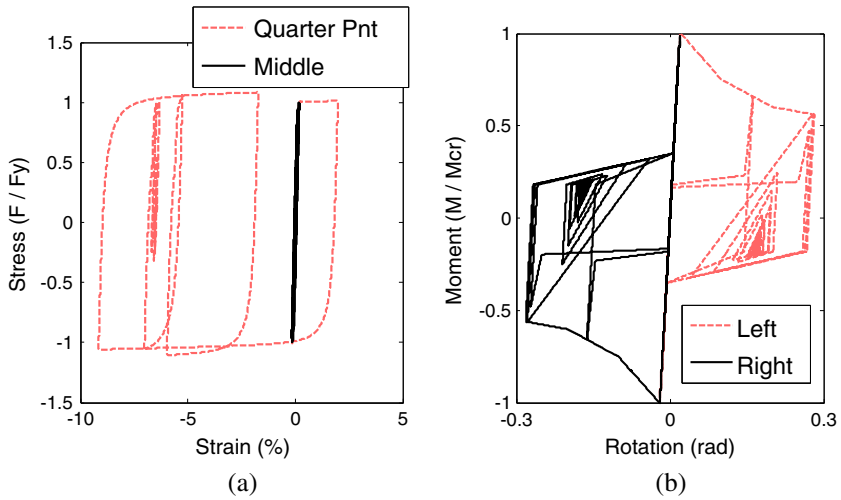

Figure 17. Behavior of fuse computational model for Specimen A6 subjected to maximum considered earthquake motion.

DOI: 10.1002/eqe

indentions or other damage was found. Although the column base details performed well in allowing uplift and pivoting of the column without observable damage, tolerances allowed some sliding of the rocking frames. As shown in Table II, the second trial for Specimen A6 experienced a residual roof drift of 0.1% that was due to sliding of the rocking frames between the bumpers. Some tolerance was required between the bumpers and the rocking frame to facilitate the desired erection sequencing. However, as described in Eatherton and Hajjar [4], in further tests, shims were added between the bumper and rocking frame, which eliminated the sliding.

6.3. Summary of peak and residual drifts

A summary of all the peak roof drifts and residual roof drifts are tabulated in Table II including predictions from the computational model. The accuracy of the computational model in predicting peak drifts was found to be better for the nondegrading fuses. The tabulated residual roof drifts given in Table II clearly show that the self-centering rocking steel frame system is capable of essentially eliminating residual drift after very large earthquake ground motions including consideration of the destabilizing P-Δ effects and ambient building resistance. These results are consistent with the findings of a companion set of shake table tests that were conducted at the E-Defense facility in Miki, Japan [3] in which the rocking steel frames were shown to exhibit negligible residual drifts and focused structural damage in replaceable fuse elements after being subjected to numerous large earthquake ground motions.

7. CONCLUSIONS

The self-centering rocking frame system consists of concentrically braced steel frames that are allowed to rock relative to the foundation with vertical post-tensioning that closes the uplifting gap thus creating a restoring force and steel butterfly fuse plates that dissipate seismic energy. A large-scale hybrid simulation testing program was conducted including six tests on two specimens. Through all of the hybrid simulation tests, the frame and post-tensioning remained elastic, demonstrating that the system could be repaired after a large earthquake by replacing the fuse plates. It was shown that nondegrading butterfly fuse plates are capable of undergoing multiple large ground motions without deterioration of their strength or stiffness. It is therefore concluded that nondegrading butterfly fuses that are designed to limit their peak fuse shear strain to 15%, which is half the magnitude that caused fracture in a separate testing program, that the fuse plates may not need to be replaced after one or two large earthquakes.

The residual drifts after every hybrid simulation test were near zero. It is concluded that the self-centering rocking steel frames are therefore capable of excellent self-centering ability. The resistance of the rest of the building was considered in the hybrid simulation through computational components simulating the resistance of steel gravity framing and interior partitions. It was found that the resistance of the rest of the building degrades significantly and with it the resistance to self-centering degrades. At the same time, the resistance of the rest of the building also acts to reduce peak drifts. The peak and residual roof drift ratios for Specimen A6 considering the resistances of the rest of building were 1.4% and 0.0%, respectively when subjected to an MCE level ground motion, demonstrating relatively small peak drifts while not causing residual drifts. Although this is based on one prototype building configuration, a larger computational study in Eatherton and Hajjar [23] found that the resistance of the rest of the building can cause significant reduction in peak drifts (by as much as 2.5 times for the range of configurations investigated), whereas residual drifts increased, but remained relatively small (less than 0.25% for the residual roof drift ratio).

Based on hybrid simulation tests, it has been shown that the self-centering rocking steel frames can satisfy enhanced seismic performance objectives as compared with conventional systems related to targeted structural repair and are thus expected to experience less business downtime and repair costs. The self-centering rocking frame system satisfies these performance objectives by concentrating all inelasticity in replaceable fuse elements and virtually eliminating residual drift.

DOI: 10.1002/eqe

ACKNOWLEDGEMENTS

This material is based upon work supported by the National Science Foundation under Grant No. (CMMI-0530756), the American Institute of Steel Construction, Stanford University, and the University of Illinois at Urbana-Champaign. In-kind funding was provided by Tefft Bridge and Iron of Tefft, Indiana, MC Detailers of Merrillville, Indiana, Munster Steel Co. Inc. of Munster, Indiana, Infra-Metals of Marseilles, Indiana, and Textron/Flexalloy Inc. Fastener Systems Division of Indianapolis, Indiana. The authors thank research collaborators Greg Deierlein, Helmut Krawinkler, and Sarah Billington; graduate students, Xiang Ma, Kerry Hall, Alejandro Pena, Eric Borchers, and Paul Cordova; practicing structural engineers, David Mar and Gregory Luth; and our Japanese collaborators for their contributions to this research. The LBCB Operations Manager and LBCB Plug-in used in this research were developed by Narutoshi Nakata, Matt Eatherton, Oh Sung Kwon, Sung Jig Kim, and Curtis Holub with support from NEES@UIUC, Grant No. A6000 SBC NEES OMSA-2004, and the Mid-America Earthquake Center, NSF Grant No. EEC-9701785. Any opinions, findings, and conclusions or recommendations expressed in this material are those of the authors and do not necessarily reflect the views of the National Science Foundation or other sponsors. [Correction made here after initial online publication.]

REFERENCES

1. Bradley BA, Curbinovski M. Near-source strong ground motions observed in the 22 February 2011 Christchurch earthquake. *Seismological Research Letters* 2011; **82**(6):853–865.
2. Ma X, Borchers E, Pena A, Krawinkler H, Billington S, Deierlein GG. Design and behavior of steel shear plates with openings as energy dissipating fuses, blume earthquake Eng. Center TR #173, Stanford University, 2010.
3. Ma X, Krawinkler H, Deierlein GG. Seismic design and behavior of self-centering braced frame with controlled rocking and energy dissipating fuses, blume earthquake Eng. Center TR #174, Stanford University, 2011.
4. Eatherton MR, Hajjar JF. Large-scale cyclic and hybrid simulation testing and development of a controlled-rocking steel building system with replaceable fuses, Report No. NSEL-025, Newmark Structural Engineering Laboratory Report Series, Univ. of Illinois at Urbana-Champaign, Urbana, Illinois, 2010.
5. Nakaki S, Stanton J, Sritharan S. An overview of the PRESSS five-story precast test building. *PCI Journal* 1999; **33**(2):26–39.
6. Priestley MJN, Sritharan S, Conley JR, Pampanin S. Preliminary results and conclusions from the PRESS five-story precast concrete test building. *PCI Journal* 1999; **44**(6):42–67.
7. Kurama YC, Pessiki S, Sause R, Lu L-W. Seismic behavior and design of unbonded post-tensioned precast concrete walls. *PCI Journal* 1999; **44**(3):72–89.
8. Holden T, Restrepo J, Mander JB. Seismic performance of precast reinforced and prestressed concrete walls. *ASCE Journal of Structural Engineering* 2003; **129**(3):286–296.
9. ACI ITG. *Acceptance Criteria for Special Unbonded Post-Tensioned Precast Structural Walls Based on Validation Testing*. ACI ITG-5.1-07, American Concrete Institute, 2007.
10. ACI ITG. *Requirements for Design of a Special Unbonded Post-Tensioned Precast Shear Wall Satisfying ACI ITG-5.1 and Commentary*. ACI ITG-5.2-09, American Concrete Institute: Farmington Hills, MI, 2009; 25.
11. Panian L, Steyer M, Tipping S. Post-tensioned concrete walls for seismic resistance. *Journal of the Post-Tensioning Institute* 2007; **5**(1):7–16.
12. Luth GP, Sargunuraj S, Krawinkler H, McDonald B. USC school of cinema – an example of repairable performance-based design. *SEAOC 2008 Convention Proceedings* 2008; 20.
13. Clough RW, Huckelbridge AA. Preliminary experimental study of seismic uplift of a steel frame. Earthquake Engineering Research Center (EERC) Report No. UCB/EERC-77-22, 1977.
14. Pollino M, Bruneau M. Analytical and experimental investigation of a controlled rocking approach for seismic protection of bridge steel truss piers, Technical Report MCEER-08-0003, 2008.
15. Midorikawa M, Azuhata T, Ishihara T, Wada A. Shaking table tests on seismic response of steel braced frames with column uplift. *Earthquake Engineering and Structural Dynamics* 2006; **35**:1767–1785.
16. Wada A, Yamada S, Fukuta O, Tanigawa M. Passive controlled slender structures having special devises at column connections. *7th International Seminar on Seismic Isolation, Passive Energy Dissipation and Active Control of Vibrations of Structures*, Assisi, Italy, October 2–5, 2001.
17. Sause R, Ricles JM, Roke DA, Chancellor NB, Gonner NP. Seismic performance of a self-centering-rocking concentrically-braced frame. *Proceeding of the 9th U.S. National and 10th Canadian Conference on Earthquake Engineering*, Toronto, Ontario, Canada, Paper No. 1330, July 25-29, 2010.
18. Wiebe L, Christopoulos C. Mitigation of higher mode effects in base-rocking systems by using multiple rocking sections. *Journal of Earthquake Engineering* 2009; **13**(S1):83–108.
19. MacRae GA, Kawashima K. Post-earthquake residual displacements of bilinear oscillators. *Earthquake Engineering and Structural Dynamics* 1997; **26**(7):701–716.
20. Ruiz-Garcia J, Miranda E. Residual displacement ratios for assessment of existing structures. *Earthquake Engineering and Structural Dynamics* 2006; **35**:315–336.
21. Christopoulos C, Pampanin S, Priestley MJN. Performance-based seismic response of frame structures including residual deformations, part I: single-degree of freedom systems. *Journal of Earthquake Engineering* 2003; **7**(1): 97–118.

DOI: 10.1002/eqe

22. Pettinga D, Christopoulos C, Pampanin S, Priestley N. Effectiveness of simple approaches in mitigating residual deformations in buildings. *Earthquake Engineering and Structural Dynamics* 2007; **36**(12):1763–1783.
23. Eatherton M, Hajjar JF. Residual drifts of self-centering systems including effects of ambient building resistance. *Earthquake Spectra* 2011; **27**(3):719–744.
24. Gupta A, Krawinkler H. Seismic demands for performance evaluation of steel moment resisting frame structures. John A. Blume Earthquake Engineering Center Report Number 132, 1999.
25. ASCE/SEI 7-05. Minimum design loads for buildings and other structures. Published by the American Society of Civil Engineers (ASCE), Prepared by the Structural Engineering Institute of ASCE, 2010.
26. Mazzoni S, McKenna F, Scott MH, Fenves GL. Open system for earthquake engineering simulation user command-language manual, OpenSees version 2.0, Pacific Earthquake Engineering Research Center, University of California, Berkeley, CA, 2009.
27. Kwon O-S, Nakata N, Park K-S, Elnashai A, Spencer B. UI-SIMCOR user manual and examples for UI-SIMCOR v2.6 and NEES-SAM v2.0, 2007. available from NEES Forge website: http://neesforge.nees.org/
28. Liu J, Astaneh-Asl A. Cyclic testing of simple connections including effects of slab. *Journal of Structural Engineering, ASCE* 2000; **126**(1):32–39.
29. Gad EF, Chandler AM, Duffield CF, Stark G. Lateral behavior of plasterboard-clad residential steel frames. *Journal of Structural Engineering, ASCE* 1999; **125**(1):32–39.
30. Combescure D, Pegon P. α-operator splitting time integration technique for pseudodynamic testing error propagation analysis. *Soil Dynamics and Earthquake Engineering* 1997; **16**:427–443.
31. Seo C-Y, Sause R. Ductility demands on self-centering systems under earthquake loading. *ACI Structural Journal* 2005; **102**(2):275–285.

DOI: 10.1002/eqe